Synthesis and Characterization of Graphene and Molybdenum Disulfide based multilayered 2D Nanomaterials for EMI Shielding Analysis

By

Hafiz Muhammad Sajid

School of Chemical and Materials Engineering (SCME)

National University of Sciences and Technology (NUST)

May 2022

Synthesis and Characterization of Graphene and Molybdenum Disulfide based multilayered 2D Nanomaterials for EMI Shielding Analysis

Hafiz Muhammad Sajid

Reg No: 00000275319

This thesis is submitted as a partial fulfillment of the requirements for the degree of

MS in Materials and Surface Engineering

Supervisor Name: Dr. Muhammad Irfan

School of Chemical and Materials Engineering (SCME)

National University of Sciences and Technology (NUST)

May 2022

Dedication

With the true sense of my feelings mind and heart, I dedicated this thesis to my parents, teachers, and friends.

Acknowledgement

All glory to Almighty Allah for His countless blessings that enabled me to complete my research work and thesis.

I am thankful to my loving and caring family for their valuable prayers, support, recommendations, and encouragement. I also appreciate my supervisor's advice and encouragement. I’m thankful to my supervisor because of his efforts and guidance

Hafiz Muhammad Sajid
Reg No.00000275319

Abstract

It is still very challenging to effectively design the nanocomposites microstructures which significantly improve their electromagnetic interference shielding effectiveness (EMI SE). Herein, we developed a facile method for fabrication of graphene nano platelets/Molybdenum disulfide GNPs/MoS_2 nanocomposites, in which GNPs are utilized as highly effective electrical transport materials while MoS_2 resolves the agglomeration problem of GNPs along with serves as an efficient cluster of electrical transport systems and dampens the incoming electromagnetic wave. There are two types of samples are synthesized and compared in context of EMI SE values. Physically mixed composites and layered. The sandwiched MoS_2 with GNPs layered film shows an EMI SE of 24.4 dB which is almost 14% improvement relative to GNPs/MoS_2 nanocomposites containing 0.5 wt.% GNPs exhibit an EMI SE value of 21.01dB. This work provides a new strategy for the design of multi-functional nanocomposites for EMI shielding for future applications.

Table of Contents

List of Figure

List of Tables

List of Abbreviations

XRD	X-ray Diffraction
AFM	Atomic force microscopy
SEM	Scanning electron microscopy
GNPs	Graphene Nanoplatelets
EMI	Electromagnetic Interference

Chapter 1 Introduction and literature survey

Electronics are everywhere, from autonomous vehicles to space technology in recent times. As a result, electromagnetic (EM) pollution is a brand-new kind of pollution. [1, 2]. Electromagnetic interference (EMI) in electrical devices is a common problem that, if not properly addressed, can cause system damage. Medical gadgets suffer from EMI which can cause injury to the user and prevent the device from achieving the desired outcomes[3]. EMI can momentarily disable a piece of technology and if left unprotected for a long period of time can cause irreparable damage. As a result, it is critical to ensure that all electronic devices are appropriately protected from interference. To resolve this issue of EMI, new materials and designs which can effectively absorb these EM waves must be developed.

Metal shielding is the most typical approach for EMI protection. Metals have the capability of absorbing and reflect waves, removing all emissions and providing electronic shielding. However, experiments are being conducted to see whether lightweight materials like carbon nanotubes, graphite microfiber, and metal oxides such as ZnO, CuS, MnO, Fe_3O_4, NiO/SiC, and Fe_3O_4@TiO_2[4-9] could be used to replace the metals. Molybdenum disulfide is a transition metal chalcogenide, with a layered structure comparable to that of graphite, has gained lot of consideration because of its semiconducting properties[10].

TheEM absorbing fabric has currently gained Lots of interest because of its remarkable and enticing mechanical, chemical, and physical characteristics. Molybdenum Disulfide (MoS_2) has potential applications in different regions such as super capacitors anodes, high-performance sensors, vitality change, light emitting gadgets, and in hydrogen emission[11]. MoS_2Also showed great dielectric mismatch and has a lean and large specific surface region that might effectively increment the endangering way of EM wave's interior test Conjugation of $MoS_2$with graphene nanoplatelets (GNPs) can viably increment the electrical conductivity due to the near contact between MoS_2 and GNPs leads to stable junction for charges mobility.

A MoS_2-GNPs nano composite may give more interfaces and favorable polarization centers for a mismatch of occurrence EM compared with single MoS_2 or GNPs. In

recent times various researcheshas been carried out on the improvement of due to its lower graphene oxide and dependence on grapheme for electromagnetic wave retention noteworthy characteristics. In terms of conductivity, agglomerated nanocomposites have non-uniform electrical conductivity characteristics, Figure 1-1.

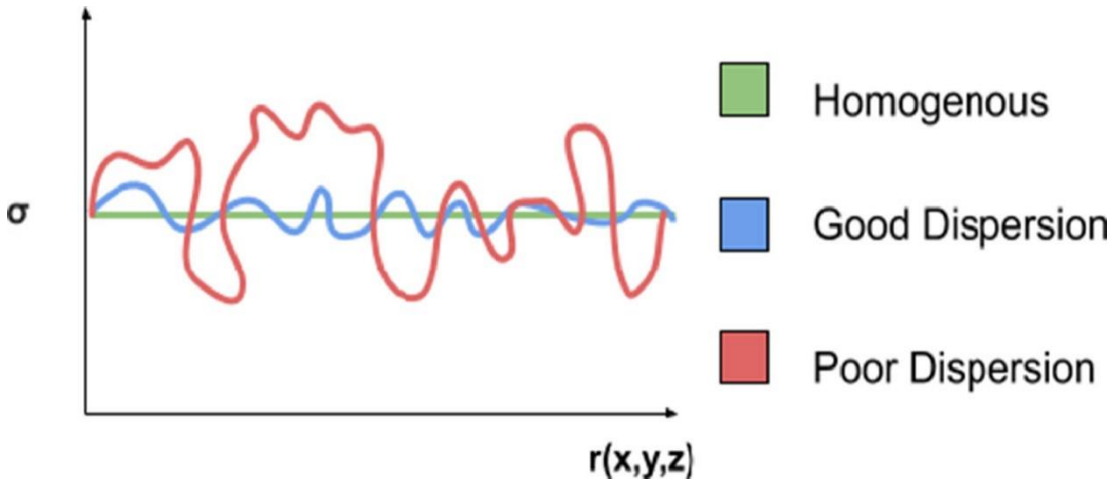

Figure 1-1Comparison of the conductivity of homogeneous, evenly dispersed, and unevenly dispersed materials using graphics [1]

Theory of electromagnetic shielding

When an electromagnetic wave strikes a conducting item, electrons are stimulated and surface current is created. For a brief period of time, material that is trapped on an object's surface is transported by surface currents. The object will either absorb or reradiate the energy[12].

A shield is essentially a metal divider in the space between two places. The objective of this metallic shield is to electromagnetically isolate these two sections (i.e., the transmission of electromagnetic waves between these two places is halted because of this metallic shield). There are two ways to employ the metallic shield. One option is to contain the source within the shield, preventing the electromagnetic field from escaping. The alternative option is to use a shield to protect the receiver/equipment so that the electromagnetic field does not interfere with it [13].Figure 1-2shows both these configurations.

The source, the medium around it, and the distance from the source all affect the electromagnetic field's characteristics.As we go away from the source, the electromagnetic field's characteristics are influenced by the medium the wave is travelling through, while the electromagnetic field's characteristics close to the source are defined by the source. As a result, two areas—near-field and far-field—can be distinguished in the medium around the source.[13].

By resolving the four equations that make up Maxwell's equations, one may examine electromagnetic waves. [14].

$$\nabla \times \vec{E} = -\frac{\partial \vec{B}}{\partial t}$$

$$\nabla \times \vec{H} = J + \frac{\partial \vec{D}}{\partial t}$$

$$\nabla . \vec{D} = \rho$$

$$\nabla . \vec{B} = 0$$

E is Electric field, ρ is charge density, B is Magnetic field, J is current density, t is time D is Electric displacement and H is Magnetic field strength.

Electromagnetic compatibility (EMC) refers to a system's capacity to work in its expected electromagnetic environment while maintaining a predetermined degree of safety and efficiency without experiencing intolerable degradation due to interferences[15].

The process by which electromagnetic disturbances are communicated from one electronic device to another either throughradiations orconductive channels or both is known as electromagnetic interference (EMI)[16]. EMI energy is reduced or eliminated via shielding (or filtering). Susceptibility is a measure of a system's proclivity to be disrupted or harmed by EMI exposure[17]. It demonstrates a lack of protection. Protection is a measure of a system's ability to withstand electromagnetic energy. Electrostatics is the study of the transmission of electric charge between objects with varying electrostatic potential when they are close to one another or come into direct contact.

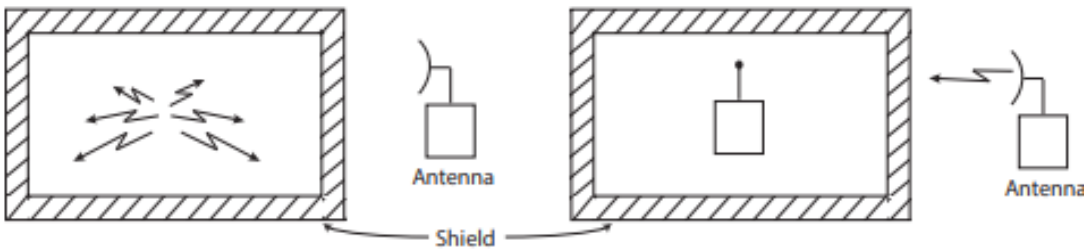

Figure 1-2 Shielding application for shielded source and receptor.

Materials used for EMI Shielding

Polymer based Composites with metal and metal oxide

Composite materials mixing various types of polymeric materials and nanoparticles of metal oxide/metal have been investigated and shown to improve EM shielding efficacy.Turczyn et al[18]explained the production of EMI shielding conductive epoxy resins including polyaniline (PANI) andpolypyrrole(PPy) components. The synthesized composite materials demonstrated good performance in the 35–30 MHz frequency band, where diminishing was the greatest, with an average difference of around 20 dBV/m between conductive and non-conductive composites. Conducting Ag nanoparticles (NPs) have been used in EMI shielding applications using a variety of polymers and copolymers[19].

For increased EMI shielding, various carbon derivative materials have been identified.Gupta et al[20]reported the addition of zinc oxide (ZnO) nanorods has effect of EMI shielding in the X-band and also nickel zinc ferrite to amorphous carbon. Cucumbers were calcined at 800°C for 1 hour to extract amorphous carbon under argon atmosphere. The EMI SET of the 1 mm thick composite material was 25.70 dB, but the addition of nickel zinc ferrite powder increased it to 53 dB.

Graphene/carbon-based materials

Graphene-based nanocomposites have been extensively researched for EMI shielding. The investigation of stretched graphene nanosheets (GNS) producing barrier walls in melamine sponge by Guo et al. [21]for excellent EMI shielding. By using a fluid-assisted technique, the GO nanosheets covered with melamine sponge pores were utilized, followed by freeze-drying and reduction procedures. The composite foam had a density of 0.011 g/cm^3, an EMI SE of 37.2 dB, and a specific EMI SE of 845.5 dB·cm^2/g with a graphene loading of 0.1 vol. percent. Song and Fan et al[22] investigated the EM shielding properties of flexible multilayer graphene sheets with high conductivity and found the effective EM shield equal to 27 dB. Guo and Zhongming et al [23]et al reported the biomass derived carbon and iron oxide based with good EM wave absorption characteristics.

Graphene/carbon-polymer composites

To provide effective EMI shielding, polymers are regarded to be an useful matrix for distributing graphene compounds.Liang et al[24]developed the ground-breaking study on functionalized graphene submerged in an epoxy matrix (in-situ technique) for improved EMI shielding materials.. The percolation threshold of functionalized graphene/epoxy composites was 0.52 volume percent graphene. A 15.0weightpercent functionalized graphene loading provided a maximum EMI SE of 21 dB in the X-band. Zhang et al.[25] reported sulfonated reduced less defect graphene oxide (S-rLGO) combined with P(St-BA) latexthrough blending and casting processes and reported an overall shielding effectiveness of 16 dB.

Jiang et al.[26]developed flexible, light-weight composite foam-based EMI materials using thermoplastic polyurethane (PU) and rGO as well as supercritical CO2 foaming. The composite's significant flexibility and excellent interfacial adhesion were made possible by hydrogen-bond interactions and in-situ GO reduction by l-ascorbic acid. The creation of a segregated structure in thermoplastic PU/rGO composites was claimed for the improved electrical conductivity. The SE of 21.8 dB was reached with only 3.17 vol. percent rGO loading due to the conductive cellular network construction.Guo et al.[27]studied the rGO@barium titanate (BT)/poly(vinylidene fluoride) (PVDF) composite and concluded that this composite can exhibit EMI SE_R(reflection) of 23dB with filler loading of 25 wt.%.

Different 2D-structured graphene and carbon nanotubes along with polymers to form 3D graphene/CNT composites have been investigated of high EMI shielding capabilities. Gupta et al[28] disclosed solvent mixing and ball milling approach for the manufacture of MWCNT/graphene/PANI nanocomposites. Graphene served as a bridge between PANI and MWCNTs in the synthesized multilayer material. By increasing the MWCNT content, the EMI SE was improved, with composites containing 10% MWCNTs obtaining an EMI SET value of 98 dB.Huangfu et al[29] studied the PANI, MWCNTs, and thermally annealed graphene aerogels dispersed in an epoxy polymer for its EMI shielding capabilities. The prepared composite exhibited high EMI shielding effectiveness of 42 dB with high mechanical strengths.Zhang et al [30] functionalized the polymethylmethacrylate (PMMA) with

graphene by foaming with subcritical $CO_2$and demonstrated a EMI shielding effectiveness in the range of 13-19 dB with graphene loading of 1.8% by volume.

MoS_2-basedmaterials

The EMI shielding of MoS_2-rGO/Fe_3O_4 nanostructure was assessed in 8-12 GHz rangeby Prasad et al [31] and EMI shielding effective $SE_T$with this material was 8.27 dB. MoS_2-rGO composite showed inadequate shielding capacity (SE_T 3.81 dB) across the entire spectrum of EM studied. Interfacial polarization played vital role in dielectric losses along with other loss mechanisms. In another report Prasad reported EMI SE in the 29-46 dB range usingCo@MoS_2/rGO nanocomposites synthesized through autoclave methods. Guo et al [32]explored rGO@MoS_2/PVDF nanocomposite for EMI shielding applications and demonstrated that the composite can reach a maximum shielding efficiency of 28 dB with 25 wt.% loading of the fillers.Ding et al [33] also recently investigated the rGO-MoS_2-Fe_3O_4 and found that the reflection loss of hydrothermal prepared composite was -48 dB.

Table 2shows different frequency bands and ranges of EMI shielding for different applications ranging from low frequency EM shielding for traffic control to high frequency EM shielding for cruise control applications.

Table 1 EMI SEof various reported materials.

Sr. no	Author	Material	Year	Fabrication/Synthesis Method	dB Ranges	Reference
1	Ding et al	rGO-MoS_2-Fe_3O_4	2021	Hydrothermal technique	-48 dB (reflection)	[33]
2	Prasad et al	Co@MoS_2/rGO	2020	Autoclave	29-46 dB	[34]
3	Muhammad Zahid	RGO/ TPU	2020	Solution casting technique	53 dB	[35]
4	Shakir et al	PS/PANI blends	2020	Solution casting method	45dB	[36]
5	Zhang et al.	S-rLGO/P(St-BA) latex	2020	Blending and casting	16 dB	[25]
6	Ramsha Khan	Graphene and MoS_2	2020	Blending and filtration	18 dB	[37]
7	Prasad et al	MoS_2-rGO and MoS_2-rGO/Fe_3O_4 nanostructure	2019	Hydrothermal method	3.81 dB (MoS_2-rGO) and 8.27 dB (MoS_2-rGO/Fe_3O_4)	[31]
8	Guo et al.	GO nanosheets covered with melamine sponge	2019	Fluid-assisted method	37 dB	[21]
9	Shakir et al	PVC/PANI/TRGO	2019	Hydrothermal technique and solution casting methods	56 dB	[38]
10	Zhang et al	Graphene/ PMMA nanocomposite	2018	foaming with subcritical CO_2	13-19 dB	[30]
11	Guo et al	rGO@BT/poly(vinylidene fluoride) (PVDF)	2017	Physical mixing and drop casting	22 dB	[27]

12	Guo et al	rGO@MoS_2/PVDF	2016	Blending and hot molding	28 dB	[32]
13	Liang et al	15% functionalized graphene/epoxy resin	2009	In-situ functionalization	21 dB	[24]

Table 2Frequency bands and ranges of EMI shielding for different applications.

Frequency Band	Frequency Spectrum (GHz)	Applications
L band	1-2	Traffic control
S band	2-4	Log range weather
C band	4-8	Airborne weather detection
X band	8-12	Short range missile guidance
Ku band	12-18	Satellite altimetry
K band	18-27	Water vapors
Ka band	27-40	Airport surveillance
V band	40-75	Scientific remote sensing
W band	75-110	Automobile cruise control

Problem Statement

Increasing the real part of the complex permittivity, ε^ ", which is linked to the absorption of EM waves, is the key to efficient EMI shielding. Multiple polarization mechanisms, including electronic, ionic, dipolar, and space charge polarization, are responsible for the rise in [39-42]. Since, ionic and electronic contributions dominate at low frequency regimes, therefore key to enhance of ε''at high EM wave frequencies will be to enhance interface and dipolar polarizations. Various interface design strategies have been adopted to increase space charge polarization which are usually complex [39-41]. In this study we have adopted simple strategy was adopted where void free compact layered structures of 2D GNPs and MoS_2nanosheets were fabricated by simple and cost-effective vacuum filtration method. Two design strategies were adopted to fabricate these layered structures. One strategy involved single layer of physically mixed composite materials of GNPs and MoS_2 with varying loadings and the other one considered the bi- and tri-layer structures of these materials where each layer composed of single type of 2D materials. The sandwich construction, i.e., tri-layer structures, showed enhanced EMI shielding effectiveness due to more space charge polarization losses along with other type of losses because of multiple interfaces. These layered constructions could be used in many fields, such as flexible electronics, automobile industry and space technologies.

Objectives

- Synthesis of 2D nanomaterials of molybdenum disulfide and graphene nano-platelets (GNPs) through Solution processing technique and fabrication of layered structures by vacuum filtration.
- Morphological and compositional studies of synthesized materials
- EMI Shielding and dielectric studies of layered structures

Chapter 2 Experimental

2.1 Materials

Bulk MoS_2 and we bought some graphite powder from Jiangsu Xfnano Materials Tech Co.Ltd. China, N-methyl-2-pyrrolidone (NMP) and nylon filter papers with pore size of 0.45 µm were obtained from Sigma Aldrich.

2.2 Synthesis of 2D materials

First 2D materials of MoS2 and graphene were prepared from bulk materials by exfoliation in NMP. For the synthesis of 2D nanosheets of MoS_2, 2 grams of MoS_2were mixed in 100 ml of NMP and dispersed by magnetic stirring for 45 min. After that the dispersion was probe sonicated (Figure 2-1)for 64 hours using 40% amplitude are 0.3 cycle. This 00ml dispersion was equally distributed in 6 centrifuge tubes which were subjected to centrifugation, first at 1500 rpm for 45 min, to exfoliate the MoS2. The sediments were stick to the walls of these tubes and the supernatants were transferred to another set of 6 tubes which were further centrifuged for 45 min at 1000 rpm.After that supernatant were transferred again into 6 new centrifuge tubes and centrifuged for 45 min at 500 rpms subsequently the exfoliated dispersions were poured into the vacuum filtration assembly. After filtration through 0.45 µm nylon filter paper, the filtered cake was removed from the filtration assembly and dried overnight in vacuum oven at temperature 60 ℃. Once dried, the MoS_2 was scratchedfrom the nylon filter paper and was used for layered structure fabrication and further testing.

Similar procedure was used to prepare graphene nanoplatelets by exfoliation of bulk graphene powder in NMP.

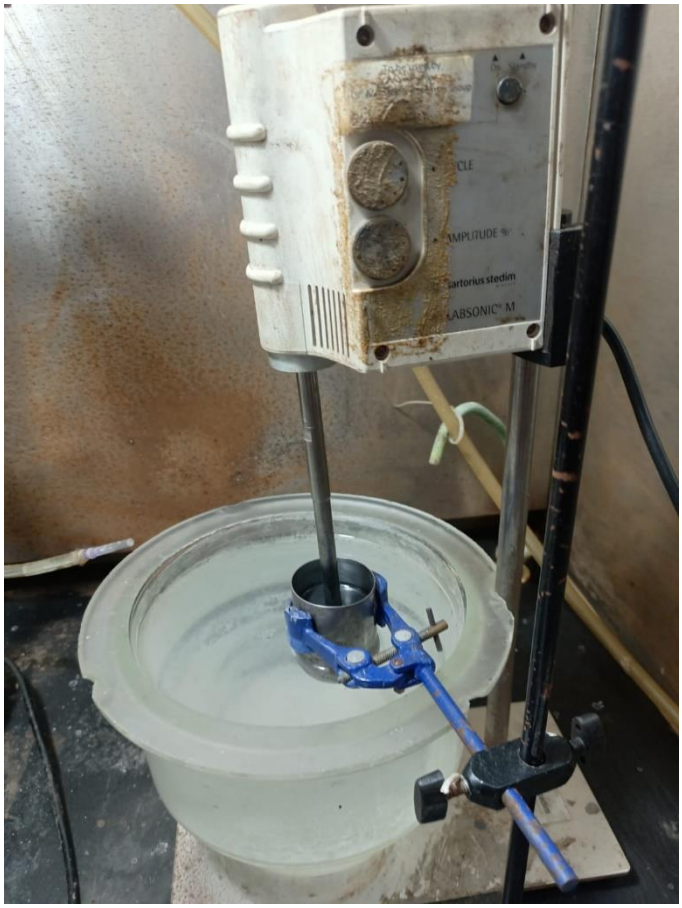

Figure 2-1 Probe Sonicator.

2.3 Layered structure fabrication by Vacuum filtration

Vacuum filtration was used to fabricate layered of synthesized 2D materials. Two design strategies were adopted: first strategy involved single layer structure containing physically mixed nanocomposites of 2D materials and the second one dealt with the bi- and tri-layered structures where instead of nanocomposites each layer was composed of single 2D material. The overall loading of 2D materials in all layered structures, single-, bi- and tri-layered ones, was kept constant, i.e., 6mg. The required amount of 2D materials, for each layer, was dispersed in 12 ml of 1:1 ratio ethanol-water solution in an ultrasonic bath for 30min and then filtered through the nylon paper by vacuum suction. The loading and sequence of layers are given Table 1. The single layer structures were fabricated by physically mixing 0%, 50%, 75%, & 100% MoS2 nanosheets with graphene platelets in ethanol-water solution and then filtering each dispersion through the nylon filter paper by suction. The filtered cakes were dried in oven at 60 °C for one hour.Figure 2-2 shows schematic of the process of layered structures'fabrication.

In bilayer structures, the first layer was fabricated by dispersing 3mg of MoS_2 in ethanol-water solution followed by vacuum suction through nylon filter paper. The filtered cake was dried in oven at 60 °C for one hour. Subsequently this dried cake was again loaded into the vacuum filtration assembly and a dispersion containing 3mg of graphene platelets was filtered through it to fabricate the second layer. The filtered cake was again dried in oven at 60 °C. A similar procedure was adopted for the fabrication of tri-layered structures where 25% of each 2D materials was sandwiched between the two layer of the other material, Table 1.Figure 2-3 shows the actual fabricated samples.

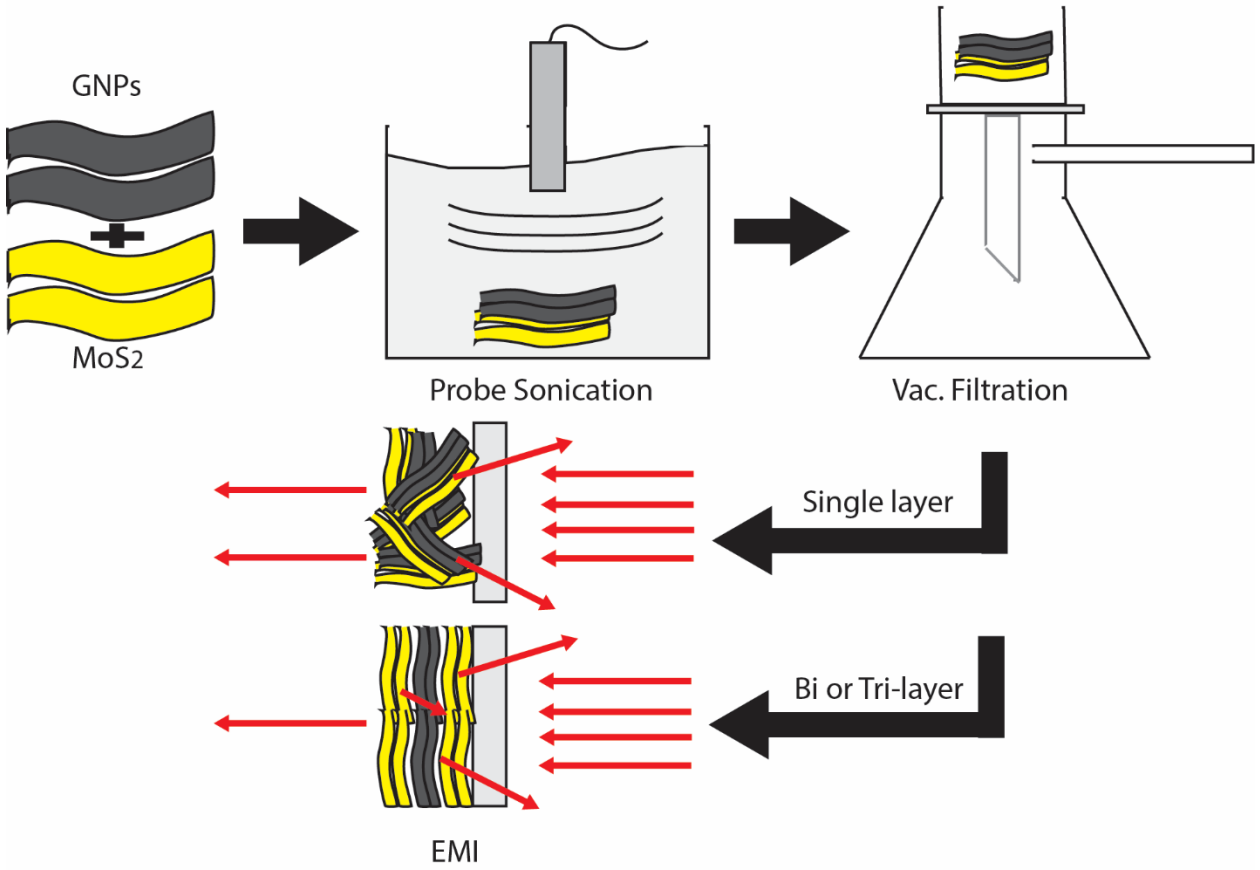

Figure 2-2 Scheme for the fabrication of layered structures for EMI shielding.

Table 3 Sample designation for single-, bi-, and tri-layer structures.

Structure	**Composition and sequence of layers in a structure**	**Sample/structure designation**
Single layer	6mg graphene	6G
	3mg MoS_2 and 3mg graphene	3MS-3G
	4mg MoS_2 and 2mg graphene	4MS-2G
	6mg MoS_2	6MS
Bilayer	3mg MoS_2/3mg graphene	3MS/3G
Tri-layer	2mg MoS2/2mg graphene/2mg MoS2	2MS/2G/2MS
	2mg graphene/2mg MoS2/2mg graphene	2G/2MS/2G

Figure 2-3Samples for EMI studies.

Chapter 3 Characterizations

3.1 Scanning electron microscopy(SEM)

The surface morphologies of synthesized samples were analyzed using Scanning electron microscopy (SEM) (JEOL-JSM- 6490LA). and SEM model VEGA FESEM equipped with Bruker EDX at CASEN- NUST. The pictures of SEMs used in this study are given in, Figure 3-1.

Figure 3-1Scanning electron microscope equipped with EDS at SCME (left)and at USPCASE, (right) NUST.

The required analysis performed bySEM with following conditions:

- Sample was sputtered using gold
- Working distance of 10mm
- 10-20 kV of operating voltage
- Current 90mA

3.2 X-ray diffraction (XRD)

A nondestructive method for examining the crystalline phases present in the test sample is X-ray diffraction. Cathode tube (X-ray source), sample holder, and X-ray detector make up the XRD machine.Figure 3-2. Electrons are generated by heating the filament in x-ray tube and accelerated towards the Cu-target. These electrons collide with the electrons in the target material and generate vacancies in the atoms. When electrons form higher energy level jumps to the lower ones, X-rays are generated. These X-rays are directed towards the sample and where they interact with the sample either constructively or destructively. The x-rays which interact with the sample according to Bragg's law, produce intensity maxima are at the detector. XRD gives information about the phases and crystallinity.XRD used in this study was (D8, Advance Bruker) present in USPCASE, NUST,Figure 3-3.The crystal structure of the prepared powder materials was probed using X-Ray Diffraction (XRD, STOE Siemens D5005) with CuKα radiations ($\lambda = 1.54$ A) operating at a voltage of 40 kV and a working current of 40 mA.The samples were subjected to a step scan of 0.04^{o} and a scan rate of 1.00 s.

3.3 Atomic Force Microscopy (AFM)

AFM is the most valuable and versatile technique to study materials at nanometer scale. It is a type of scanning probe microscopes (SPMs). AFM uses force of attraction and repulsion to 3D image a sample. It is used to obtain aspect ratio and thickness of sample material. The image is obtained by the raster scan of AFM tip over the specified area of sample. In this technique the tip is attached to a cantilever [43].

As AFM works on the interatomic forces (van der Waals forces) during the raster scan, when tip reaches toward sample surface, tip deflects toward sample surface due to attractive forces and when it reaches near surface repulsive forces generated as both sample and tip come close together. The deflections of the cantilever are measured to acquire image resolution with AFM. The optical lever mirrored the laser towards the cantilever. The mirrored laser beam hits a detector comprising of four-section detector (photo). The changes in signals between the segments of photodetector indicate angular deflections of the cantilever as shown in figure.

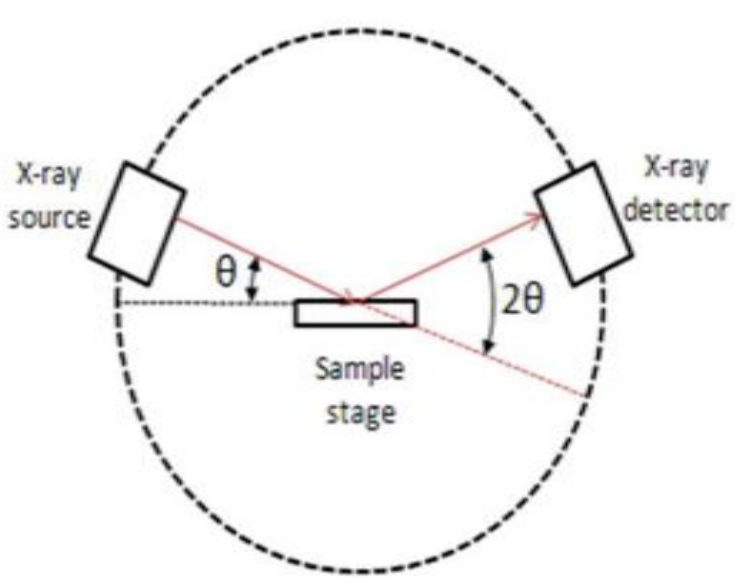

Figure 3-2 XRD setup.

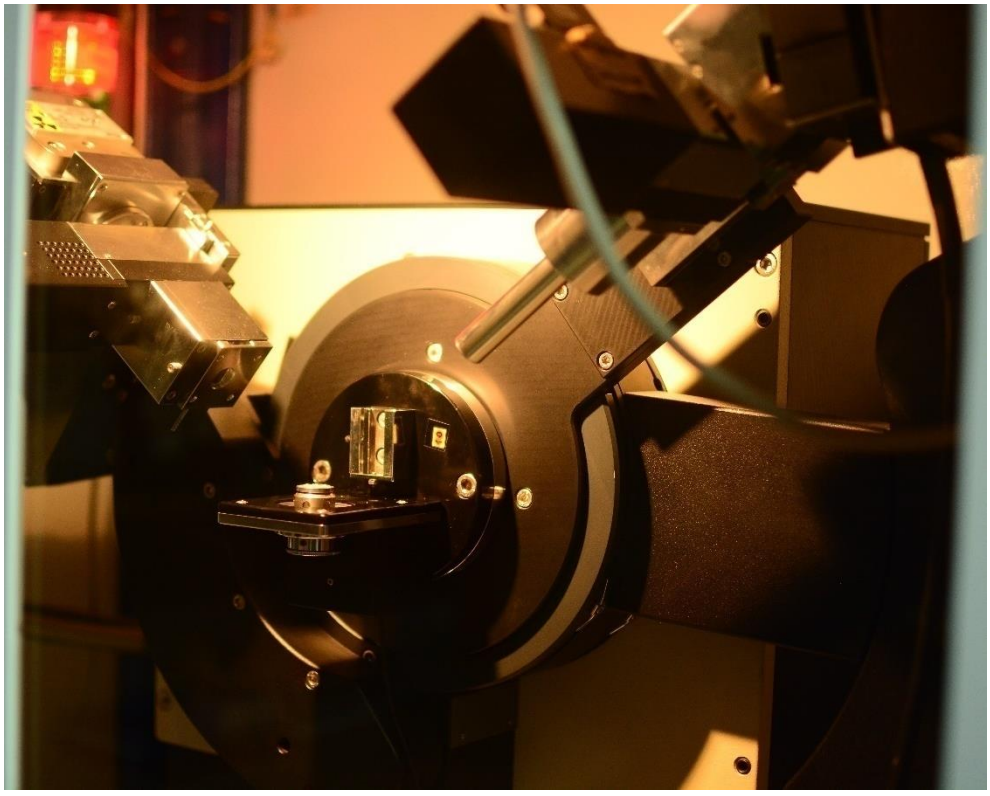

Figure 3-3 XRD machine

The AFM images was obtained by JOEL JSPM-5200, Figure 3-4. The samples were prepared by preparing a solution of samples in deionized water and then drop casted on glass slide and dried. The length, height and aspect ratios were studied using AFM images.

Figure 3-4 Atomic force microscope.

3.4 RAMAN Spectroscopy

Raman spectroscopy is vibrational spectroscopy in which light interacts with the molecule to change the polarizability of molecule. Raman Effect was first discovered by C.V.Raman and K.S. Krishnan in 1928. The technique was then become a powerful tool to analyze chemical substances. When the light of specific wavelength is focusedon the molecule, the photons are scattered elastically and inelastically. Elastic scattering is termed as Rayleigh scattering. A portion of photons from the incident beam (1 in 107 photons approx.) are scattered inelastically, called Raman effect, having lower energy (and frequency) than that of the incident photons [44]. Raman scattering is caused by a change in the molecule's electrical, rotational, or vibrational energy. Stokes shift is a phenomenon where the dispersed photons have less energy than the incident photons. Since the small population is already in a vibrationally excited state, upon Raman scattering the molecule is then relaxed back to the ground state lower than the initial state, therefore the Compared to the incident photon, the emitted photon has a higher energy and a shorter wavelength. The Anti-Stokes shift is the name of this phenomenon. At room temperature, the anti-Stokes shift spectrum is always dimmer than the Stokes shifted Raman spectrum. both have the same frequency information, therefore Stokes-shifted Raman spectrum is usually observed [34]. Figure 3-5 shows all these effects with electronic energy states.

The fundamental parts of a Raman spectrometer are a laser excitation source, excitation delivery optics, a sample, collection optics, a wavelength separation device, detector and associated electronics, and a recording device. A Raman spectrum is a graph of the Raman scattered radiation's intensity as a function of the Raman shift, or the difference in frequency between the scattered and incident radiation (units of wavenumbers, cm^{-1}). Raman spectroscopy is an important technique used to study solids (particles, pellets, powder, films, and fibers), liquid (gels, pastes) and gases in the area of biochemistry to material sciences [45, 46].

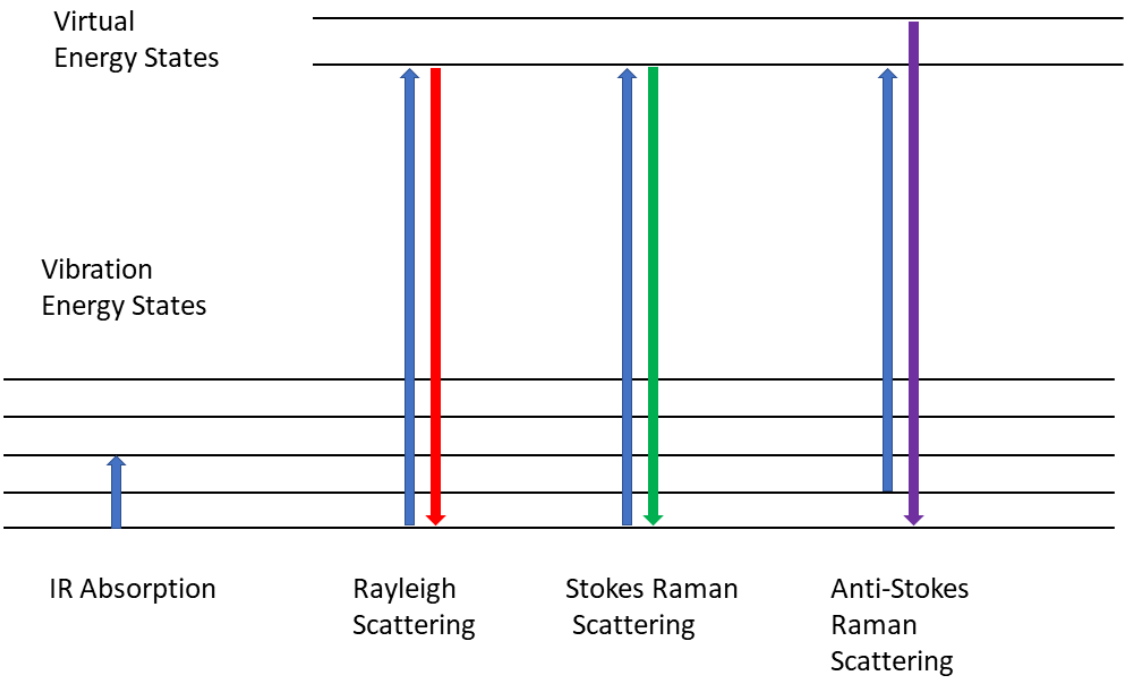

Figure 3-5Rayleigh scattering, Stokes Raman, and anti-Stokes Raman scattering energy level diagrams

3.5 EMI shielding

Electrical conductivity and magnetic permeability of materials, as well as the frequency of radiation, play a vital influence in EMI shielding. The effectiveness of theshielding material is ratio of incident power (P_I) to transmitted power (P_T) through the shield, as given by Eq.:

$$EMISE(dB) = 10\log\frac{P_I}{P_T}$$

EMI testing for prepared samples were carried out at PNA Model E8364B. The data is obtained as scattering parameters which are combination of transmission and reflection responses. These scattering parameters are called S-parameters. Which are S_{11}, S_{12}, S_{21} and S_{22}.

$$Reflectance(R) = \frac{P_R}{P_I} = {S_{11}}^2 = {S_{22}}^2$$

$$Transmittance(T) = \frac{P_T}{P_I} = {S_{12}}^2 = {S_{21}}^2$$

The total EMI SE (SET) is the sum of the contributions from the shielding effect reflection (SER), the shielding effect absorption (SEA), and other internal reflections (SEM). At higher EMI SE values and with a multilayer EMI shield, the contribution from many internal reflections is integrated into the absorption because the re-reflected waves are converted into heat in the shielding material.The total EMI SE (SE_T) is the sum of the contributions from refection (SE_R), absorption (SE_A) and multiple internal reflections (SE_M)

$$SE_T = SE_R + SE_A$$

Where both SE_A and SE_R are as followed,

$$SE_R = 10\log\frac{1}{1-{S_{11}}^2}$$

$$SE_A = 10\log\frac{1-{S_{11}}^2}{{S_{21}}^2}$$

Microwave reflection happens when there is an impedance mismatch between the surface of the shielding material and the incoming radiation. But when incoming electromagnetic wave energy is reduced, absorption takes place, and the internal inhomogeneity of the shielding material results dis recurrent reflections. It's worth noting that a SE_A of less than 10 dB is adequate to eliminate multiple reflection contributions.

The total shielding effectiveness (SE_T) is the total shielding contribution owing to the above-mentioned components, and the specifics tying it to the various scattering characteristics have been described elsewhere.

The complex permittivity properties of the synthesized materials including dielectric constant, and dielectric losses were measured with vector networkanalyzer (VNA, N5242A PNA-X, Agilent (Figure 3-6)) at room temperature in the frequency range of 1 GHz to 8 GHz. For finding the real factor of resistivity following relation was used

$$\varepsilon' = Cd/A\varepsilon_0$$

Here, ε' is the dielectric constant, C the capacitance, d the distance between the plates, and ε_0 the permittivity of free space.

For finding the imaginary factor of resistivity following equation was used, where (tanδ) is the dissipation factor

$$\varepsilon'' = \varepsilon' tan\delta.$$

3.6 Electrical properties

Dielectric properties are measured using impedance analyzer, Figure 3-7, The pellet was placed in pellet holder and connected to device for measurements.

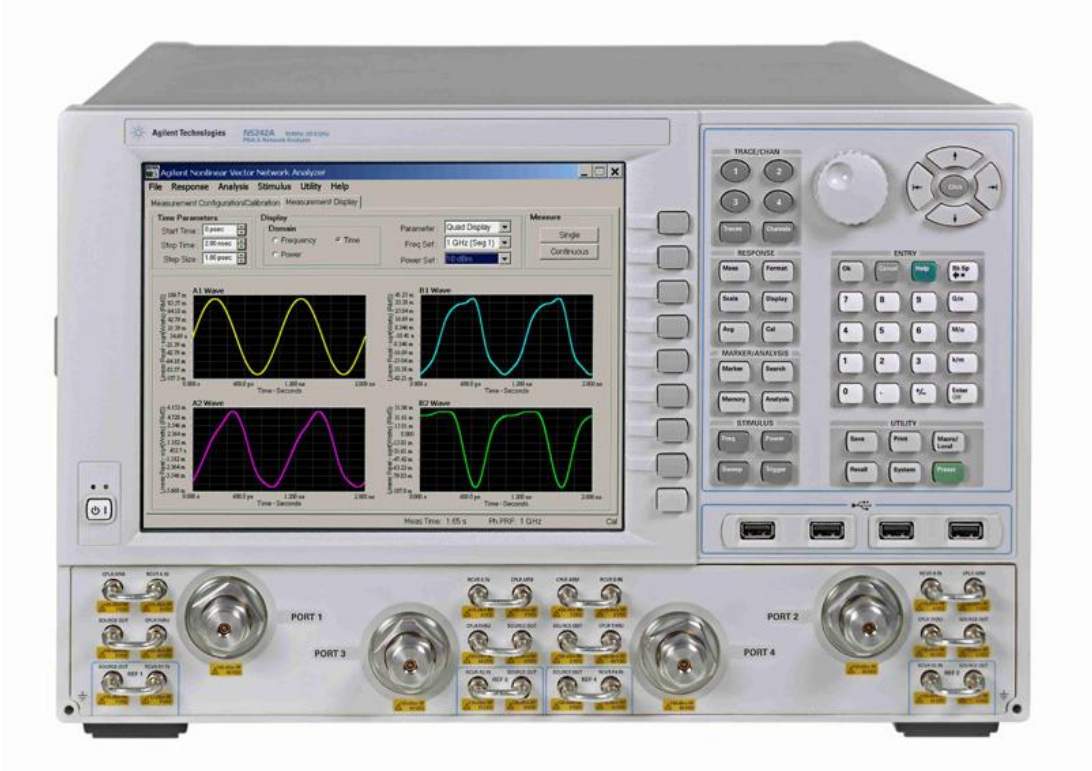

Figure 3-6VNA, vector networkanalyzer.

Figure 3-7 LCR meter

Chapter 4 Results and Discussions

4.1 Morphological and Structural Analysis

The morphologies synthesized 2D materials of GNPs and MoS_2 are shown inFigure 4-1. SEM images of synthesizes GNPs revealed triangular and rectangular forms, Figure 4-1 (A&B), with layered sheets of sizes varying between 1-5 microns and thickness in 2–10 nm ranges. A broad variety of layered agglomerates of varying shapes and number of layers were observed. There were no single or few layers sheets of graphene found.The flakes-like structures with stacking of few layers are evident from the morphological analysis of synthesized MoS_2 as shown in Figure 4-1(C &D). The MoS_2sheets were composed of clusters of various thicknesses. As reported in literature the mechanical strength between the layers of bulk MoS2 is weakened during probe sonication[47]and nanosheets of sizes ranging from 1 micron to 5 microns were obtained.

The elemental maps of single layer composite structures s are shown inFigure 4-2. The sulfur and molybdenum contents decreased with increasing content of graphene in physically mixed composite layer, Figure 4-2 A to C. The dispersion of both phases was mostly uniform in the composite layer. The big interfacial contact between MoS_2 and GNPs 2D materials was evident for 3MS-3G composition, Figure 4-2 B, compared to the other compositions (Figure 4-2 A & C).

Figure 4-3A shows the XRD patterns of graphene Nano platelets (GNPs). The characteristics peaks of graphene are evident inFigure 4-3A. A high intensity peak at a 2θ value of $26°$ was associated with (002) plane of graphite. Also, two less intense peaks at 44° and 54° are evidentFigure 4-3A which belonged to (100) and (004) planes of graphene, respectively. These characteristic peaks of GNPs matches well with PDF card 00-02-0212 given Figure 4-3B and conform with reported literature [48].

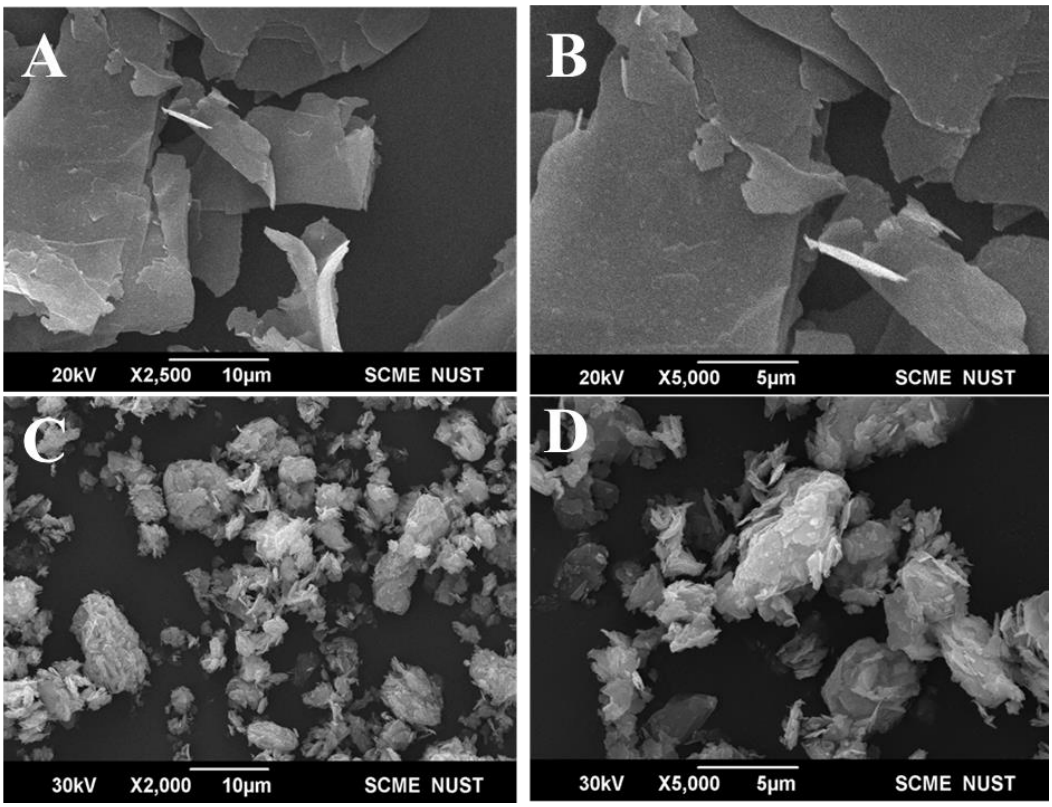

Figure 4-1SEM images of GNPs (A &B) and MoS2(C &D)

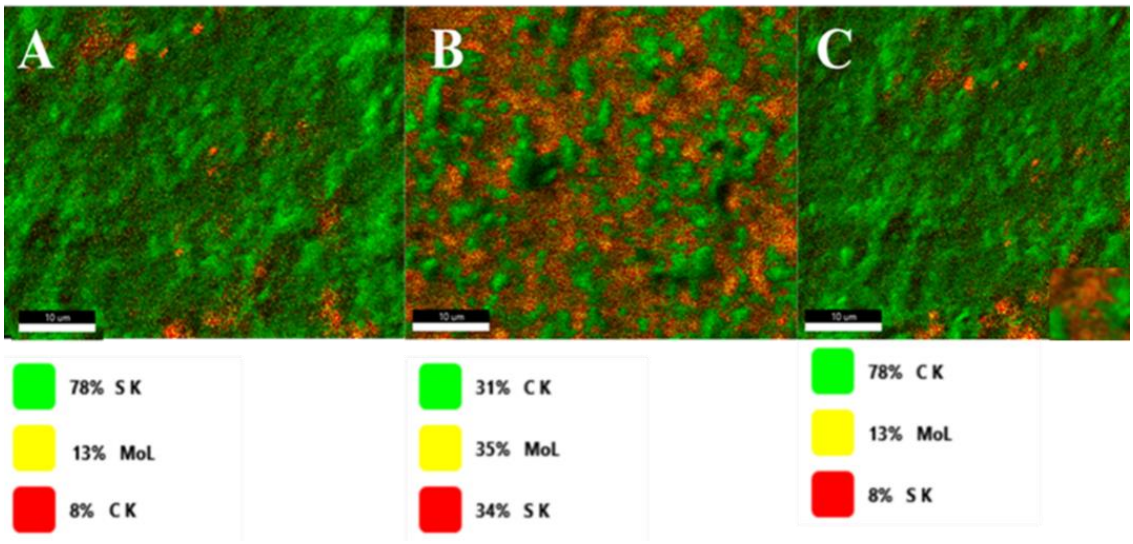

Figure 4-2Elemental mapping A) 4MS-2G, B) 3MS-3G, C) 2MS-4G

Figure 4-4 A shows the XRD pattern of MoS_2. The diffraction peaks at 14.37°, 32.67°, 35.86°, 39.53°, 44.16°, 49.76°, 58.32°, and 60.12° belonged to (002), (100), (102), (103), (104), (105), (110), and (112) planes, respectively. The observed XRD peaks of MoS_2 matched well with reference PDF card 01-077-1716 shown in figure 4-4B and with the reports.

To find the thickness and lateral length of nanosheets, the statistical analysis of AFM was done. As show in Figure 4-5the length of GNPs was around 0.2 µm and height, which shows the thickness of these nanosheets, was ~5.2 nm. Also, area roughness measurement R_a and R_z were 2.69 nm and 20.8 nm, respectively for GNPs as shown in figure 4-5. MoS_2 flakes were ~0.5 µm in length and their thickness was ~10.2 nm as shown in Figure 4-6. Similarly, for Mos2, R_a and R_z were 1.62 nm and 31.62 nm, respectively.

Raman spectroscopy is a quick way to get a direct look at electron-phonon interactions, which means it's very sensitive to electronic and crystallographic structures[49, 50]. Figure 4-7illustrates Ramanspectrum of GNPs where main band for GNPs was observed at around 1600 cm^{-1}. The Raman spectra of carbon compounds have three primary bands between 1200 and 2800 cm^{-1}. The D and G bands at 1360 $cm^{-1}$and 1600 cm^{-1}, respectively, are caused by sp^2sites while T band at 1060 cm^{-1}due to sp^3 contributions [49]. There was no D band observed for synthesized GNPs, Figure 4-7. Some literature reports suggest that the Raman spectrum would be redshifted when the graphene is subjected to strain, because of the stretch of carbon-carbon bond[51, 52].

In Figure 4-7B only first order E_{2g}^1 and A_{1g} Raman modes were observed as the incident energy was considered non resonant.These modes are often helpful in finding the number of layers of MoS_2 sheets.It has been observed from figure that the intensive peaks around 400 cm^{-1}corresponded to MoS_2 E_{2g}^1.MoS2 showed aberrant resonance Raman characteristics,Figure 4-7B, as reported[53]. The core peak and the broad peak centered at the Rayleigh scattered laser line are caused by the resonant activation of exciton states by acoustic phonon scattering.[53]. Furthermore, due to resonance with exciton or exciton-polariton states characteristics, several second order Raman peaks were observed.

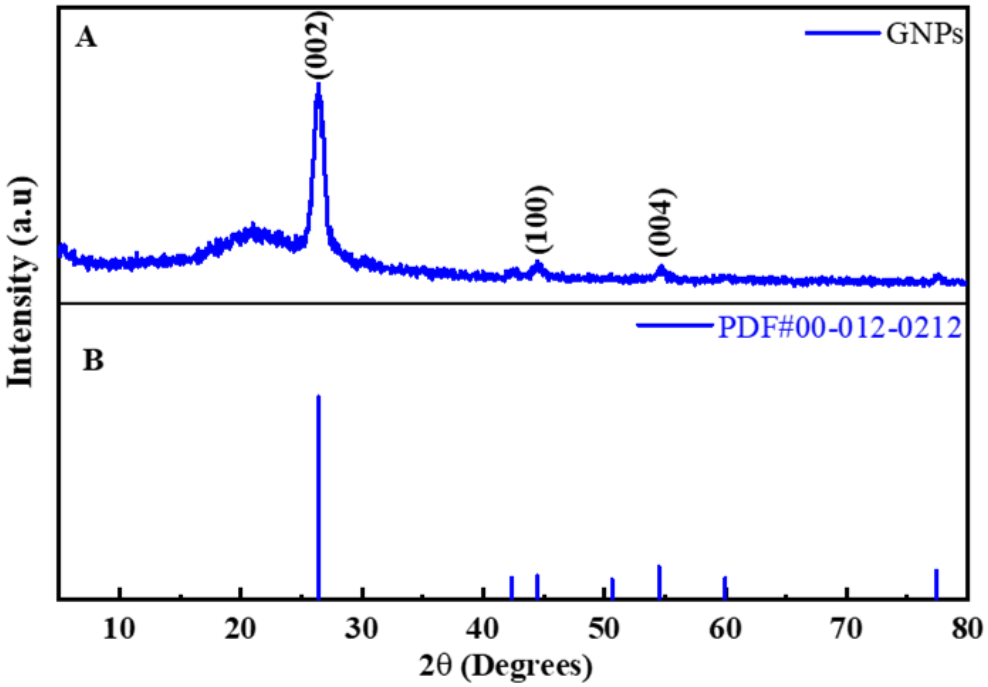

Figure 4-3a) XRD Patterns of GNPs and b) reference PDF card # 00-02-0212

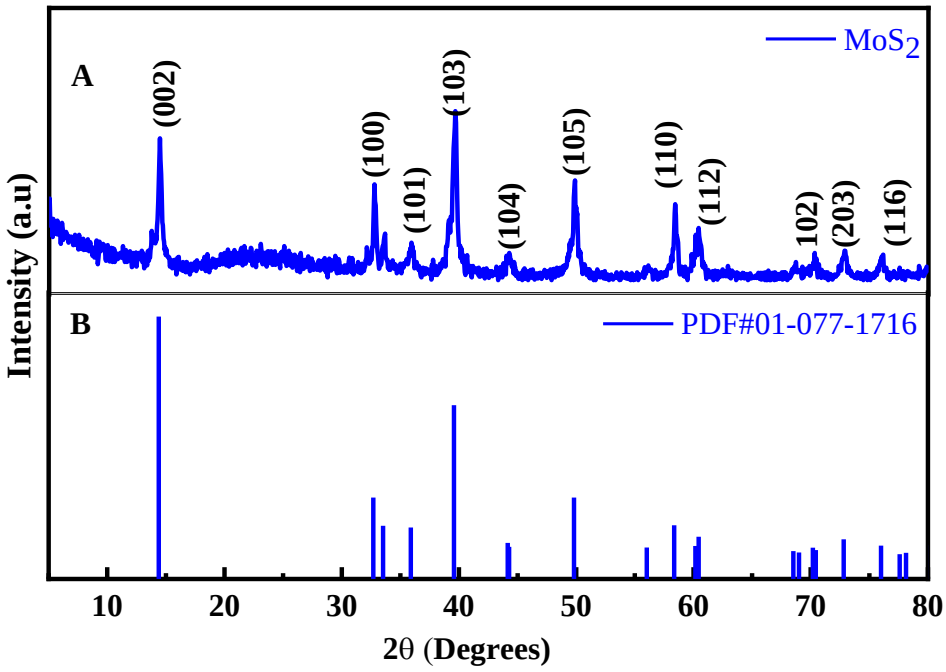

Figure 4-4A) XRD Patterns of MoS2 and B) reference PDF card 01-077-1716

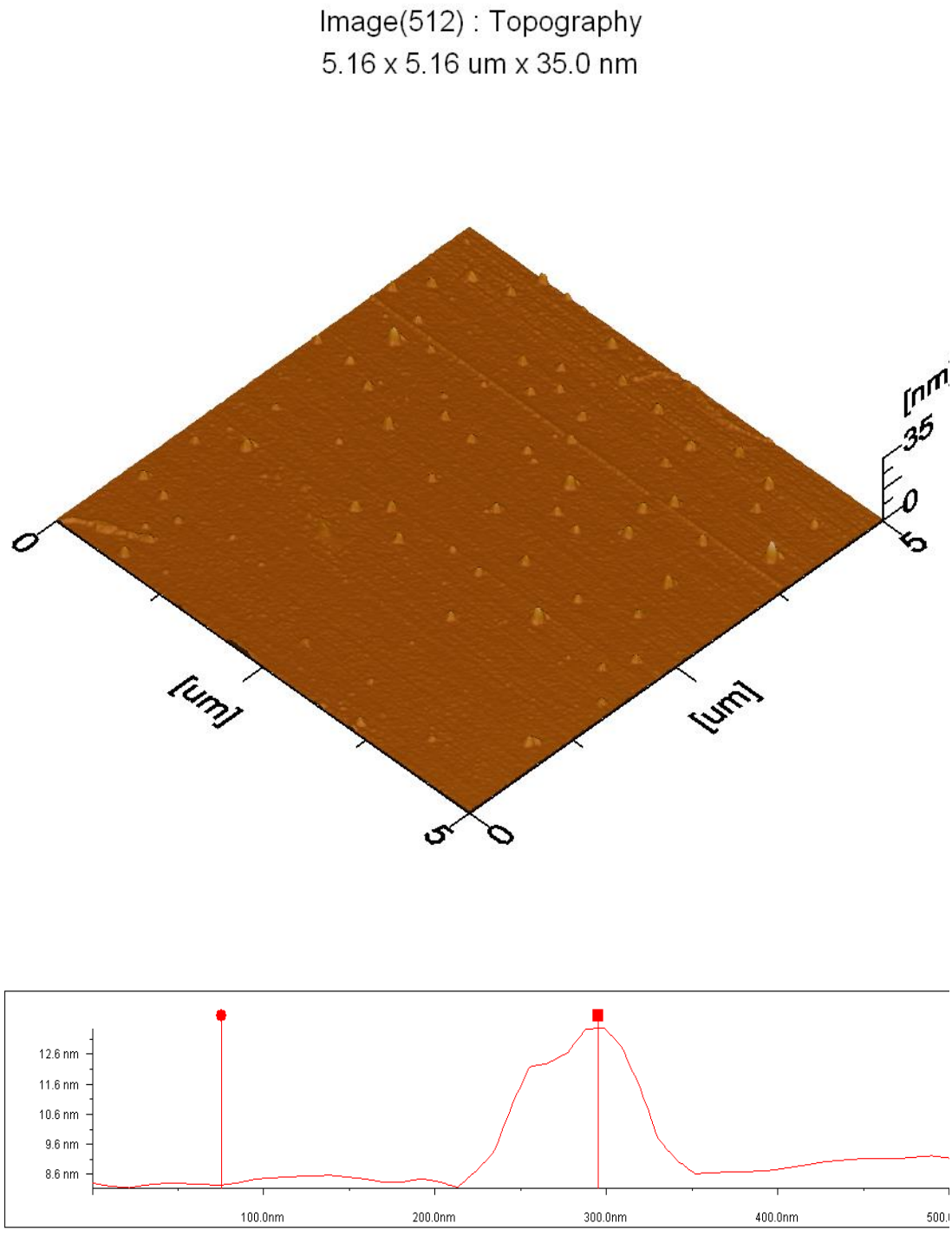

Figure 4-5 Roughness data of GNPs

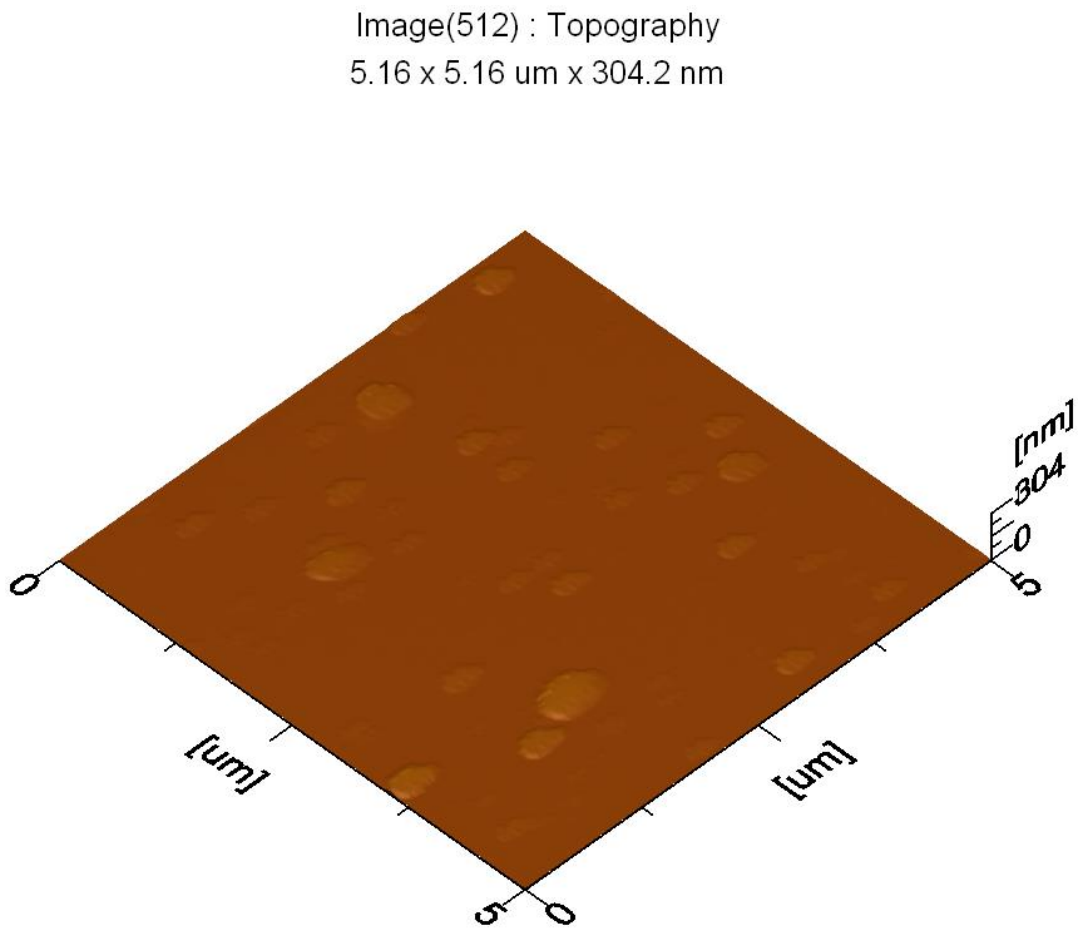

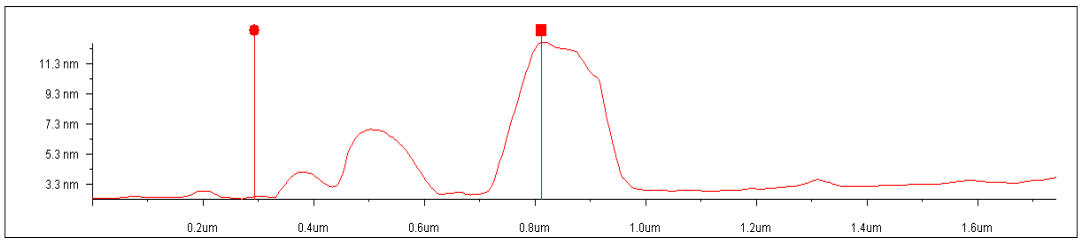

Figure 4-6Roughness data of MoS_2

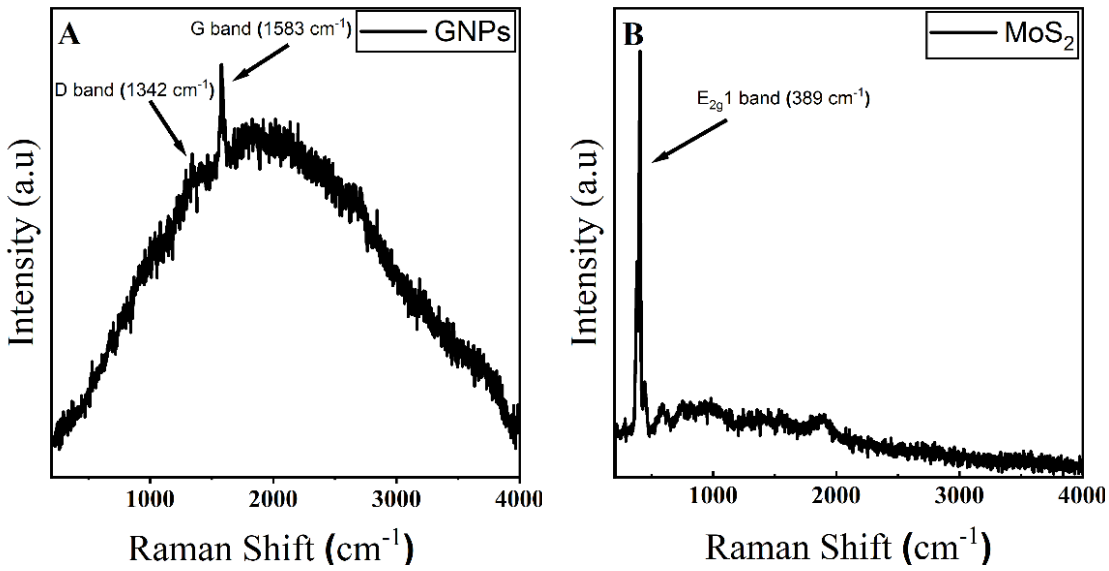

Figure 4-7 Raman scan of (A)2D GNPs (B) 2DMoS_2.

4.2 Electromagnetic Shielding Performances of Multilayer-Structure Films

The effectiveness of EMI shielding with single layer physically composite structures is shown in Figure 4-8A. The EM absorption capacities of both pristine 2D materials, i.e., MoS2 and GNPs were lower compared to their composites, Figure 4-8A.

However, pristine GNPs illustrated more EM reflection behavior compared to the pristine MoS_2which was attributed to higher electrical conductivities of GNPs compared to that of MoS_2 nanosheets. The addition of MoS_2 into GNPs or vice versa led to enhanced EM wave absorption characteristics of the resultant composite in Figure 4-8A. The maximum EMI SE was established at 50% content of each phase, i.e., 3MS-3G,where it reached a value of 21.01dB at a lower frequency of 2GHz.A drop in EMI SE was observed for all compositions at frequencies higher than 5GHz, Figure 4-8C.

As has previously been established [54], multiple polarizations such as interfacial, dipolar, ionic and electronic polarization [41, 55]and relaxation mechanisms can explain the absorption of EM waves impinging on the hybrid structures of various compositions. The electronic and atomic dipoles have a quick reaction to the alternating EM field in the GHz region and synchronize with the EM wave, resulting in no EM wave energy loss[55]. The contributions from ionic and electronic usually occur at a lower frequencies, i.e., UV or IR, therefore, interfacial and dipole polarization effects may dominate in increased EMI SE at higher frequency ranges [41].

As has been observed that the additions of GNPs in MoS_2resulted in enhanced EMI SE in Figure 4-8C, the big interface contact due to these graphene additions may have provided the platform for the polarization. Also, with high electrical conductivity, graphene sheets with a high aspect ratio tend to raise the percolation network[56]. The charge carriers get accumulated at the interfaceheterostructurecausing space charge polarization and since these charges find themselves unable to respond in accordance with the incident EM field, lead to the energy loss of EM radiation[57]. Hence, the maximum EMI SE was obtained for single layer 3MS-3G composite.

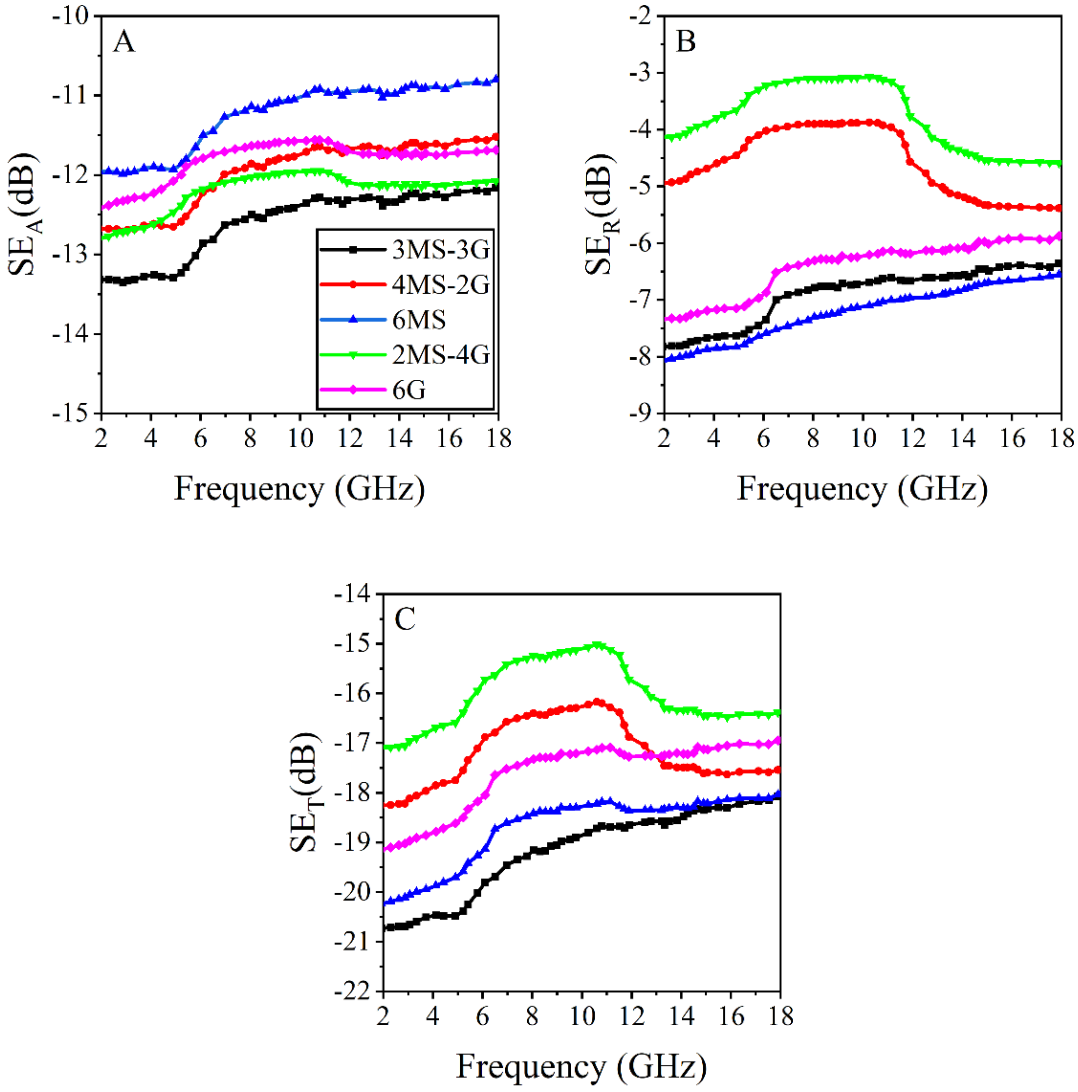

Figure 4-8 EMI SE characteristics of various single layer composite structures.

The EMI SE of the bi- and tri-layered structures was better compared to the single layered composite structures, Figure4-9. The bilayer structure, i.e., 3MS/3G, showed poor EM wav absorption and overall EM shielding characteristics compared to the

tri-layer ones, Figure4-9. In tri-layer structures, the EMI SE was maximum, i.e., 24.4 dB, when MoS_2layer was sandwiched between GNPs layers (2G/2MS/2G; Figure4-9A and was relatively lower (23.7 dB)when GNPs layerwas sandwiched between MoS_2 layers (2MS/2G/2MS; Figure4-9B. Also, EMI SE of 2G/2MS/2G was constant for the entire frequency region, Figure4-9C.

The better EM wave shielding properties of bi-layer or trilayer samples were due to multiple interfaces which might lead to space charge polarization and hence dissipation of wave energy as explained earlier. The highest EMI SE of 2G/2MS/2G can be attributed to the fact the more conductive facing layers of the sandwich structures will allow more EM waves to enter the layered structures and hence more absorption of ME waves due to conductive losses. Also, the difference in electrical conductivities between GNPs and MoS_2will result in more charge accumulation at these heterostructure interfaces and hence further energy losses due to space charge polarization. Therefore, sandwiching the insulator layer of MoS_2 in conducting layer of GNPs was a better design strategy for EMI shielding probably due to the less reflection and hence more absorption and attenuation of EM waves.

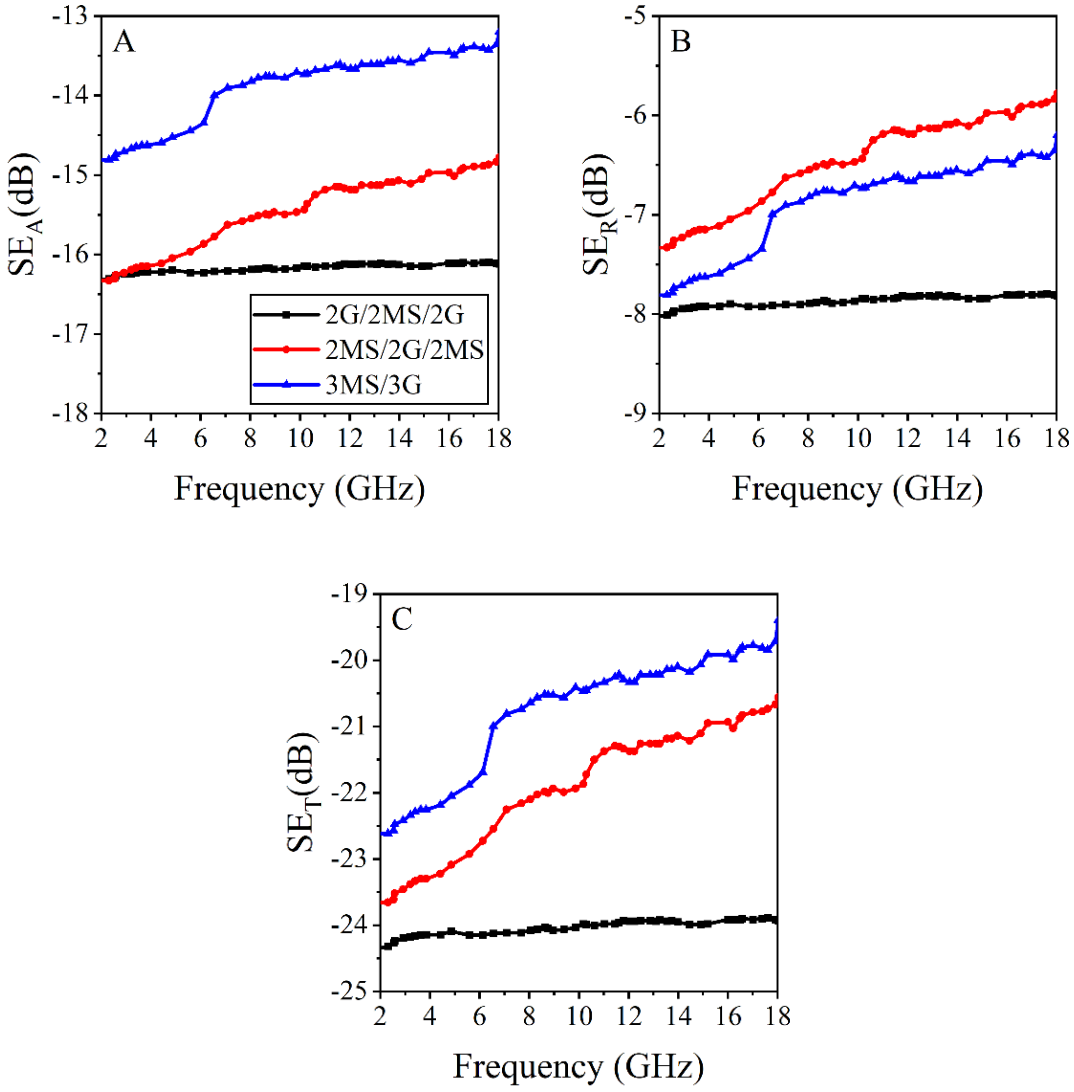

Figure4-9: EMI shielding effectiveness of bi- and tri layer structures.

4.3 Dielectric properties

The dielectric data of complex permittivity of the fabricated single layer composite structures of MoS_2 and GNPs is given in Figure 4-10 A and Figure 4-10B. This data showed the typical frequency dependent behavior and can be explained based on the Debye theory,

$$\varepsilon = \varepsilon' - j\varepsilon'' = |\varepsilon| \exp(-j\delta)$$

where, the dielectric constant (ε') is the ability of a material to store electric charge in the electric field. The imaginary part (ε''), usually referred to as the loss factor, is a material's ability to absorb or dissipate energy through conversion of electric energy into heat[41].

Figure 4-10A shows the data for real part of complex permittivity, ε', for single layer composite structures. All materials had large dielectric constants at low frequencies, but as the frequencies increased, the values of the dielectric constant decreased. Koop's hypothesis can be used to explain this tendency.; according to which dielectric structures is inhomogeneous Maxwell Wagner type[58]. The materials are composed of conducting grains separated by non-conducting boundaries. The hopping of electrons at interface because of grain boundaries in composite interface facilitates the higher primitivities.GNPs had a dielectric constant of 20 and additions of MoS_2in GNPs resulted in increase in dielectric constant, and it reached to a value of around 120 for 3MS-3G composite structure, Figure 4-10 A. Primarily, the addition of GNPs into MoS_2 was beneficial for the creation of multiple interfaces facilitating the interfacial polarization of the composites and higher dielectric permittivity. The larger surface area of MoS_2-GNPsstructures resulted in greater dipole polarization, which increased the dielectric constant. The charge at the surface of MoS_2-GNps heterostructure can drive the migration and redistribution of atoms or dipoles within material resulting in delocalization effects [28].

The increasing concentrations of MoS_2 in GNPs led to increase in complex permittivity, ε'', and maximum values of complex permittivity, ε'', at all frequencies were observed for 3MS-3G structures, Figure 4-10B. Since the contributions to complex permittivity, ε'', due to electronic and ionic polarizations mostly dominate in IR or visible regions of EM spectrum, the observed enhancement of complex permittivity, ε'', would come from dipolar and interface polarization mechanisms. The peaks in complex permittivity, ε'', versus frequency graphs are at high frequencies are usually indicative of contributions from interface polarization effect [39-41]. Therefore, heterostructure interfaces in 3MS-3G single layer composite structure resulted in higher complex permittivity, ε'', as was evident by the peaks at higher frequencies Figure 4-10B.

The tangent loss behavior of single layer composite structures is shown inFigure 4-10C. The dielectric loss was comparatively large in the lower frequency region due to the charge's mobility in the composite materials, whereas the dielectric loss was decreased in the higher frequency region due to the dipolar and interfacial polarization losses. Furthermore, in the high frequency range, a steady increase can be seen, it is because of dynamic relaxation of segmental motions in the amorphous phase, and it is called dielectric relaxation peak of dielectric loss [30].

These dielectric loss results were consistent with imaginary part and real part of dielectric constants, Table 4. The effect of concentrations of components of the single layer composite structures are evident in Figure 4-10C. GNPs had higher dielectric loss whichwas due to variable thickness and inconsistency in lateral dimensions. As the opposite case of MoS_2 2D sheets for dielectric loss. It has very less loss of dielectric constant. It has been observed that 2D MoS_2sheets have less di-polarization as compared to graphene nanoplatelets. this can play a role in low dielectric loss.

Table 4Dielectric properties of different samples at 2GHz.

Sample	**ε'**	**ε''**	**tan δ**
6MS	70.9	600.10	0.68
6G	18.5	100	0.95
3MS-3G	112.0	1100	0.52
2MS-4G	16.3	150	0.10
4MS-2G	79.7	700	0.15

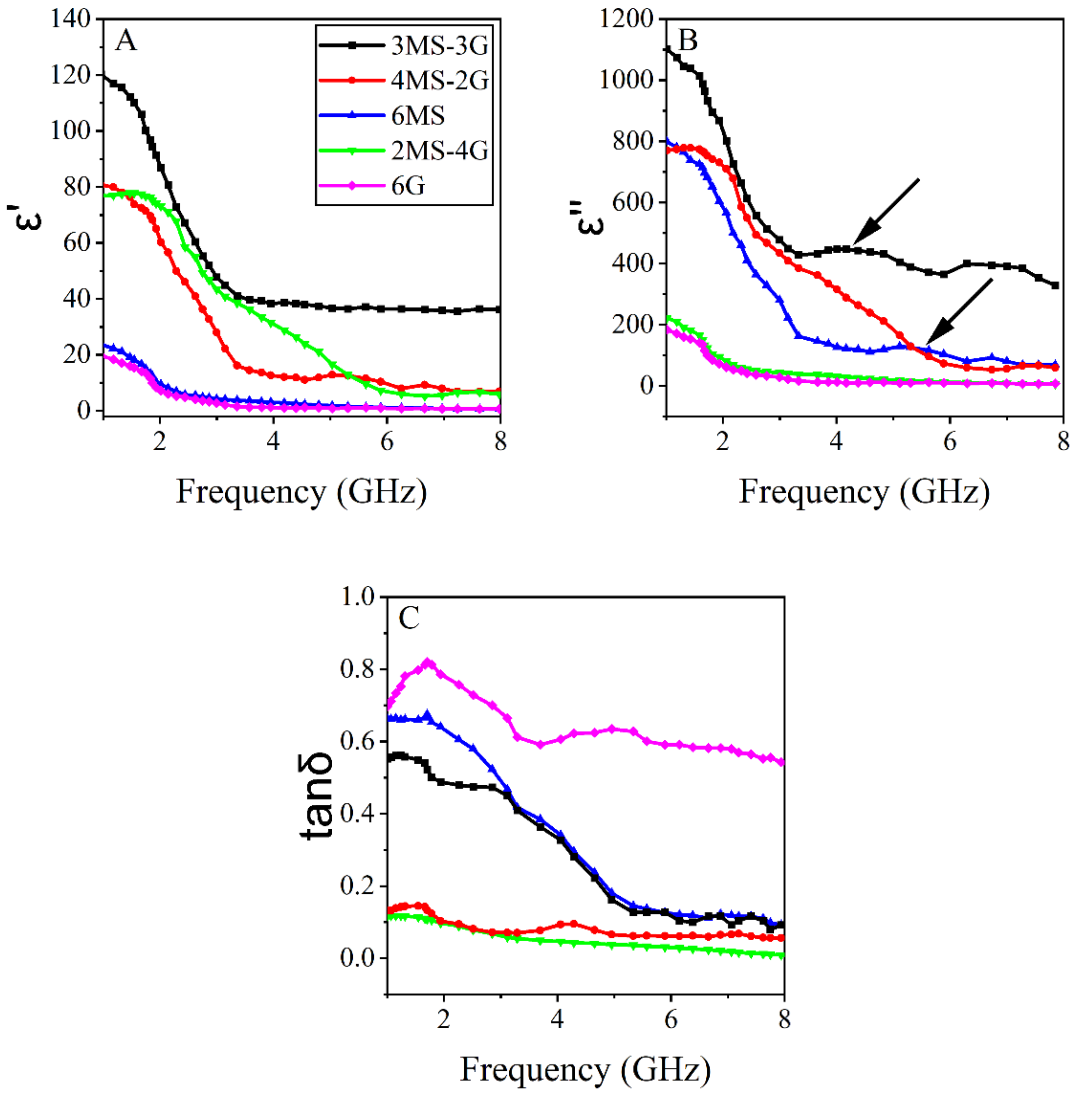

Figure 4-10 Delectric permitivity of various single layer composite structures (A) Real part (B) Imaginary part (C) Tangent loss

Conclusions

This study successfully exploited the simple low-cost vacuum filtration method for the fabrication of layered heterostructure interfaces of 2D materials of graphene and $MoS_2$to mitigate the electromagnetic interference. Initially 2D materials of MoS2 and graphene were prepared by probe sonication and centrifugation methods.

The morphological and topographical analysis of the synthesized materials using SEM and AFM confirmed 2D nature of these materials. The 2D materials were present in the form of agglomerates of varying sizes and there were on single sheets of any 2D material observed.

The EDS analysis revealed large contact at 50-50% concentration of both 2D materialsand the presence of the required elements in the synthesized materials.The structural analysis of the synthesized materials using XRD and Raman spectroscopy further elaborated their electronic and atomic structures.

Various layered structures were established by varying the concentrations of 2D materials in a single layer or by changing the order of each 2D material in bi or tri-layer structures.The heterostructures of bi or tri-layers exhibited better EMI SE with dB values reaching to 24 compared to the single layer composite structures which could be due to the multiple interfaces present in these structures because of interface polarization effectsand hence dissipation of wave energy. Along with interfacial polarization, other mechanisms such as dipolar, ionic, and electronic polarization relaxation can explain the absorption of EM waves impinging on the hybrid structures of various compositions.

The sandwiching of MoS2in GNPs layerswas a better strategy compared to thephysical mixing on these materials int a single composite layer with the same loading of each 2D material.

Future works

- The effect of thickness of layers and the number of layers on EMI SE need to be studied.Also, further studies may be carried out to see the influence of layer sequence on the EMI SE.MoS_2 with different graphene derivatives as well as other 2D materials can also be studied to check their EMI shielding effectiveness.
- The mechanical properties of these materials may be studied to check their load carrying capacities.
- Doping of other materials such as Fe_2O_3into these materials may further improve the EMI SE.
- The studied 2D materials showed remarkable electrical properties so they can be applicable in cathodes of batteries and/or super capacitors.

References

[1] Anderson, L., et al., *Modelling, Fabrication and Characterization of Graphene/Polymer Nanocomposites for Electromagnetic Interference Shielding Applications.* (2021): p. 100047.

[2] Kulkarni, G.K., et al., *α-MnO2 nanorods-polyaniline (PANI) nanocomposites synthesized by polymer coating and grafting approaches for screening EMI pollution.* (2021). **47**(11): p. 15044-15051.

[3] Mesquita, A., J. Glenn, and A.J.A. Jenny, *Differential activation of eMI by distinct forms of cellular stress.* (2021). **17**(8): p. 1828-1840.

[4] Shen, B., et al., *Lightweight, multifunctional polyetherimide/graphene@ Fe3O4 composite foams for shielding of electromagnetic pollution.* (2013). **5**(21): p. 11383-11391.

[5] Zubair, K., et al., *Effect of barium hexaferrites and thermally reduced graphene oxide on EMI shielding properties in polymer composites.* (2021). **34**(1): p. 201-210.

[6] Kruželák, J., et al., *Progress in polymers and polymer composites used as efficient materials for EMI shielding.* (2021). **3**(1): p. 123-172.

[7] Hu, X.-S., et al., *Preparation of flower-like CuS by solvothermal method for photocatalytic, UV protection and EMI shielding applications.* (2016). **385**: p. 162-170.

[8] Agarwal, P.R., et al., *Three-dimensional and highly ordered porous carbon–MnO 2 composite foam for excellent electromagnetic interference shielding efficiency.* (2016). **6**(103): p. 100713-100722.

[9] Choi, Y.-J., et al., *Characteristics of the electromagnetic interference shielding effectiveness of Al-doped ZnO thin films deposited by atomic layer deposition.* (2013). **269**: p. 92-97.

[10] Chelvanathan, P., et al., *Effects of transition metal dichalcogenide molybdenum disulfide layer formation in copper–zinc–tin–sulfur solar cells from numerical analysis.* (2012). **51**(10S): p. 10NC32.

[11] Kumar, S., et al., *Efficient electron transfer across a ZnO–MoS2–reduced graphene oxide heterojunction for enhanced sunlight-driven photocatalytic hydrogen evolution.* (2017). **10**(18): p. 3588-3603.

[12] Vargas-Bernal, R., *Performance Analysis of Electromagnetic Interference Shielding based on Carbon Nanomaterials used in AMS/RF IC Design*, in *Performance Optimization Techniques in Analog, Mixed-Signal, and Radio-Frequency Circuit Design*. (2015), IGI Global. p. 268-294.

[13] Huang, J.C.J.A.i.P.T.J.o.t.P.P.I., *EMI shielding plastics: a review.* (1995). **14**(2): p. 137-150.

[14] Monk, P., *Finite element methods for Maxwell's equations*. (2003): Oxford University Press.

[15] Violette, N., *Electromagnetic compatibility handbook.* (2013): Springer.

[16] Kaur, M., S. Kakar, and D. Mandal. *Electromagnetic interference*. in *2011 3rd International Conference on Electronics Computer Technology*.(2011). IEEE.

[17] Lun, T.J.M.A.N., *Designing for board level electromagnetic compatibility.* (2005). **2321**.

[18] Turczyn, R., et al., *Fabrication and application of electrically conducting composites for electromagnetic interference shielding of remotely piloted aircraft systems.* (2020). **232**: p. 111498.

[19] Shen, Y., et al., *Robust and flexible silver-embedded elastomeric polymer/carbon black foams with outstanding electromagnetic interference shielding performance.* Composites Science and Technology, (2021). **213**: p. 108942.

[20] Gupta, S., et al., *Hybrid composite mats composed of amorphous carbon, zinc oxide nanorods and nickel zinc ferrite for tunable electromagnetic interference shielding.* (2019). **164**: p. 447-457.

[21] Guo, T., et al., *Stretched graphene nanosheets formed the "obstacle walls" in melamine sponge towards effective electromagnetic interference shielding applications.* Materials & Design, (2019). **182**: p. 108029.

[22] Song, W.-L., et al., *Flexible graphene/polymer composite films in sandwich structures for effective electromagnetic interference shielding.* (2014). **66**: p. 67-76.

[23] Guo, Z., et al., *Magnetic coupling N self-doped porous carbon derived from biomass with broad absorption bandwidth and high-efficiency microwave absorption.* Journal of Colloid and Interface Science,(2022). **610**: p. 1077-1087.

[24] Liang, J., et al., *Electromagnetic interference shielding of graphene/epoxy composites.* Carbon, (2009). **47**(3): p. 922-925.

[25] Zhang, W., et al., *Exfoliation and defect control of graphene oxide for waterborne electromagnetic interference shielding coatings.* Composites Part A: Applied Science and Manufacturing, (2020). **132**: p. 105838.

[26] Jiang, Q., et al., *A two-step process for the preparation of thermoplastic polyurethane/graphene aerogel composite foams with multi-stage networks for electromagnetic shielding.* (2020). **21**: p. 100416.

[27] Guo, A.-P., et al., *Improved microwave absorption and electromagnetic interference shielding properties based on graphene–barium titanate and polyvinylidene fluoride with varying content.* Materials Chemistry Frontiers, (2017). **1**(12): p. 2519-2526.

[28] Gupta, T.K., et al., *Multi-walled carbon nanotube–graphene–polyaniline multiphase nanocomposite with superior electromagnetic shielding effectiveness.* Nanoscale, (2014). **6**(2): p. 842-851.

[29] Huangfu, Y., et al., *Fabrication and investigation on the PANI/MWCNT/thermally annealed graphene aerogel/epoxy electromagnetic interference shielding nanocomposites.* (2019). **121**: p. 265-272.

[30] Zhang, H.-B., et al., *Tough Graphene−Polymer Microcellular Foams for Electromagnetic Interference Shielding.* ACS Applied Materials & Interfaces, (2011). **3**(3): p. 918-924.

[31] Prasad, J., et al., *Synthesis of MoS₂-reduced graphene oxide/Fe₃O₄ nanocomposite for enhanced electromagnetic interference shielding effectiveness.* Materials Research Express, (2018). **5**(5): p. 055028.

[32] Guo, A.-P., et al., *Excellent Microwave Absorption and Electromagnetic Interference Shielding Based on Reduced Graphene Oxide@MoS2/Poly(Vinylidene Fluoride) Composites.* ChemPlusChem, (2016). **81**(12): p. 1305-1311.

[33] Ding, X., et al., *Preparation and characterization of an effective microwave absorbent: RGO-MoS2-Fe3O4 nanocomposite.* Journal of Materials Science: Materials in Electronics, 2021. **32**(7): p. 9640-9649.

[34] Prasad, J., et al., *High-efficiency microwave absorption and electromagnetic interference shielding of Cobalt-doped MoS2 nanosheet anchored on the*

surface reduced graphene oxide nanosheet. Journal of Materials Science: Materials in Electronics, (2020). **31**(22): p. 19895-19909.

[35] Zahid, M., et al., *Fabrication of reduced graphene oxide (RGO) and nanocomposite with thermoplastic polyurethane (TPU) for EMI shielding application.* Journal of Materials Science: Materials in Electronics, (2020). **31**(2): p. 967-974.

[36] Shakir, M.F., et al., *EMI Shielding Characteristics of Electrically Conductive Polymer Blends of PS/PANI in Microwave and IR Region.* Journal of Electronic Materials, (2020). **49**(3): p. 1660-1665.

[37] Khan, R., et al., *2D nanosheets and composites for EMI shielding analysis.* Scientific Reports, (2020). **10**(1): p. 21550.

[38] Shakir, H.M.F., et al., *Mechanical, thermal and EMI shielding study of electrically conductive polymeric hybrid nano-composites.* Journal of Materials Science: Materials in Electronics, (2019). **30**(18): p. 17382-17392.

[39] Liu, Y., et al., *Synthesis of MnxOy@C hybrid composites for optimal electromagnetic wave absorption capacity and wideband absorption.* Journal of Materials Science & Technology, (2022). **103**: p. 157-164.

[40] Guo, R., et al., *Tailoring Self-Polarization of BaTiO3 Thin Films by Interface Engineering and Flexoelectric Effect.* (2016). **3**(23): p. 1600737.

[41] Lv, H., et al., *Interface Polarization Strategy to Solve Electromagnetic Wave Interference Issue.* ACS Applied Materials & Interfaces, (2017). **9**(6): p. 5660-5668.

[42] Ameer, S. and I.H. Gul, *Influence of Reduced Graphene Oxide on Effective Absorption Bandwidth Shift of Hybrid Absorbers.* PLOS ONE, (2016). **11**(6): p. e0153544.

[43] Rana, M.S., H.R. Pota, and I.R. Petersen, *Improvement in the Imaging Performance of Atomic Force Microscopy: A Survey.* IEEE Transactions on Automation Science and Engineering, (2017). **14**(2): p. 1265-1285.

[44] Willard, H.H., et al., *Instrumental methods of analysis.* (1988).

[45] Robinson, J.W., E.M.S. Frame, and G.M. Frame II, *Undergraduate instrumental analysis*. (2014): CRC press.

[46] Long, D.A., *Raman spectroscopy.* New York, (1977): p. 1-12.

[47] Rahman, M.T., et al., *Structural characteristics, electrical conduction and dielectric properties of gadolinium substituted cobalt ferrite.* (2014). **617**: p. 547-562.

[48] Gutić, S., et al., *Surface charge storage properties of selected graphene samples in pH-neutral aqueous solutions of alkali metal chlorides-particularities and universalities.* (2016). **11**(10): p. 8662-8682.

[49] Ferrari, A.C. and J.J.P.r.B. Robertson, *Resonant Raman spectroscopy of disordered, amorphous, and diamondlike carbon.* (2001). **64**(7): p. 075414.

[50] Choi, W., et al., *Solid State Mater.*(2010). **35**: p. 52-71.

[51] Yoon, D., Y.-W. Son, and H. Cheong, *Strain-Dependent Splitting of the Double-Resonance Raman Scattering Band in Graphene.* Physical Review Letters, (2011). **106**(15): p. 155502.

[52] Havener, R.W., et al., *Angle-Resolved Raman Imaging of Interlayer Rotations and Interactions in Twisted Bilayer Graphene.* Nano Letters, (2012). **12**(6): p. 3162-3167.

[53] Lee, J.-U., et al., *Anomalous excitonic resonance Raman effects in few-layered MoS 2.* (2015). **7**(7): p. 3229-3236.

[54] Liu, Y., et al., *Synthesis of MnxOy@ C hybrid composites for optimal electromagnetic wave absorption capacity and wideband absorption.* (2022). **103**: p. 157-164.

[55] Karlovets, D. and A.J.a.p.a. Potylitsyn, *Universal description for different types of polarization radiation.* (2009).

[56] Worsley, M.A., et al., *Mechanically robust 3D graphene macroassembly with high surface area.* (2012). **48**(67): p. 8428-8430.

[57] Cheng, B., et al., *PMMA interlayer-modulated memory effects by space charge polarization in resistive switching based on CuSCN-nanopyramids/ZnO-nanorods pn heterojunction.* (2015). **5**(1): p. 1-9.

[58] Radoń, A., et al., *Electrical Conduction Mechanism and Dielectric Properties of Spherical Shaped Fe_3O_4 Nanoparticles Synthesized by Co-Precipitation Method.* Materials (Basel, Switzerland),(2018). **11**(5): p. 735.